

Ambient formaldehyde detection with a laser spectrometer based on difference-frequency generation in PPLN

D. Rehle^{1,*}, D. Leleux¹, M. Erdelyi¹, F. Tittel^{1,**}, M. Fraser^{2,***}, S. Friedfeld^{2,****}

¹Rice University, Department of Electrical and Computer Engineering, MS 366, 6100 Main Street, Houston, TX 77251-1892, USA

²Rice University, Department of Environmental Science and Engineering, MS 317, 6100 Main Street, Houston, TX 77005, USA

Received: 8 November 2000/Revised version: 30 January 2001/Published online: 21 March 2001 – © Springer-Verlag 2001

Abstract. A laser spectrometer based on difference-frequency generation in periodically poled LiNbO₃ (PPLN) has been used to quantify atmospheric formaldehyde with a detection limit of 0.32 parts per billion in a given volume (ppbV) using specifically developed data-processing techniques. With state-of-the-art fiber-coupled diode-laser pump sources at 1083 nm and 1561 nm, difference-frequency radiation has been generated in the 3.53- μm (2832-cm⁻¹) spectral region. Formaldehyde in ambient air in the 1- to 10-ppb V range has been detected continuously for nine and five days at two separate field sites in the Greater Houston area operated by the Texas Natural Resource Conservation Commission (TNRCC) and the Houston Regional Monitoring Corporation (HRM). The acquired spectroscopic data are compared with results obtained by a well-established wet-chemical *o*-(2,3,4,5,6-pentafluorobenzyl) hydroxylamine (PFBHA) technique.

PACS: 42.68.A; 42.62.F

High concentrations of ground-level ozone are commonly measured in many urban centers. Summertime peak concentrations in excess of National Ambient Air Quality Standards impact both human health and ecosystem welfare. New air-quality measurements that incorporate precise measurements of individual trace organic compounds involved in ozone chemistry need to be developed and used to advance the understanding of ozone formation. One of the more important species in the study of ozone atmospheric chemistry is formaldehyde (HCHO), a precursor to atmospheric ozone production, present at concentrations of 2–20 parts per billion in a given volume (ppbV) [1]. HCHO is also used as

an industrial chemical, is directly emitted from motor vehicles as a result of incomplete fuel combustion [2], and is produced by the photochemical oxidation of volatile organic compounds (VOCs). In urban environments that commonly exceed ozone standards, including Los Angeles, Atlanta, and Houston, monitoring of HCHO distribution and its daily concentration cycle is an important validation of air-quality models that simulate the complex chemistry of ozone formation.

To achieve a better understanding of the origin of formaldehyde-formation processes and degradation, methods used to quantify ambient concentrations of formaldehyde must be improved. Techniques commonly used for formaldehyde quantification rely on chemical sorption of HCHO in large air volumes with 2,4-dinitrophenylhydrazine (DNPH) and require sampling times of several hours [3, 4]. Recent advances include a measurement technique employing a Nafion membrane scrubber and fluorometric quantification which provides accurate data within a few minutes [5]. Real-time, accurate concentration measurements of formaldehyde have been made using tunable diode-laser absorption spectroscopy (TDLAS) on the fundamental ro-vibrational lines with cryogenically cooled lead-salt diode lasers operating near 2831 cm⁻¹ (3.5 μm) [6–9], Fourier-transform infrared spectroscopy (FTIR), and differential optical absorption spectroscopy (DOAS) [10, 11]. However, the complexity of these instruments and their need for cryogenic cooling have limited real-time measurements of atmospheric formaldehyde [12] with these techniques to a few expert groups worldwide.

In this work, a portable, cw, high-power gas sensor using diode-laser-pumped difference-frequency generation (DFG) is reported. This device is based on our previous efforts to develop such a mid-infrared spectroscopic source [13–16] and allows for accurate, instantaneous measurements of atmospheric formaldehyde [17]. Although DFG-based gas sensors have advantages such as noncryogenic operation, intrinsic wavelength stability, and good beam quality, which are essential characteristics for their use as portable, compact devices, their low cw power (< 5 μW) has limited their minimum

*Corresponding author.

(Fax: +1-713/348-5237, E-mail: Dirk.Rehle@gmx.net)

Present address: Friedastr. 6a, 10317 Berlin, Germany

** (Fax: +1-713/348-5237, E-mail: fkt@rice.edu)

*** (Fax: +1-713/348-5203, E-mail: mpf@rice.edu)

**** (Fax: +1-607/255-8297, E-mail: sjf4@cornell.edu) Present address: Cornell University, College of Arts and Sciences, Ithaca, NY 14850, USA

detection sensitivity to date [18]. To increase the available power of tunable infrared radiation produced in such a sensor, a DFG architecture was developed that is based on two frequency-stable diode lasers at 1083 and 1561 nm which are amplified by high power Yb and Er/Yb fiber amplifiers [19], respectively. Tunable, narrow-line-width (< 60 MHz) mid-infrared radiation can be routinely generated at power levels of up to $580 \mu\text{W}$ [20,21]. This significantly higher power capability allows the use of an optical-noise-reducing dual-beam absorption configuration that employs two DC-coupled Peltier-cooled HgCdTe (MCT) detectors and a 100-m absorption path length in a low-volume (3.3ℓ) astigmatically compensated Herriott gas cell. Seiter and Sigrist [22] reported an on-line analysis of CHCO traces near $3.53 \mu\text{m}$ with a detection limit of ~ 8 ppb using a 36-m multi-pass cell and a pulsed DFG-based spectroscopic source.

1 Experimental setup

The DFG gas-sensor configuration used in this work is depicted in Fig. 1. The two primary mixing single-frequency diode lasers are a fiber-pigtailed 2-mW 1561-nm distributed feedback (DFB) telecommunications diode laser and a fiber-coupled 50-mW 1083-nm distributed Bragg reflector (DBR) diode laser, respectively. An Er^{3+} -doped fiber pre-amplifier increases the 1561-nm seed power to 30 mW to saturate the gain in a 0.65-W Er/Yb fiber amplifier. The 1083-nm diode seeds a 50-mW Yb preamplifier, the output of which in turn saturates the gain of a 1.6-W Yb amplifier. The two pump channels are then combined into a single optical fiber using a 2-port beam combiner or wavelength-division multiplexer (WDM). The difference-frequency mixing occurs on a separate optical parametric frequency-conversion stage for practical considerations. The fiber-delivered beam is imaged by a 1-cm focal-length achromatic lens (L) into the 19-mm-long anti-reflection-coated LiNbO_3 (PPLN) crystal. A 5-cm focal length CaF_2 lens collimates the difference-frequency radiation exiting the PPLN crystal. The collimated beam obtained from the lens is divided into two beams by a ZnSe wedge. The primary beam is directed to a MCT detector located after the multi-pass cell, and the reference beam is incident onto the second MCT. This dual-beam technique allows the optical fringes that arise from etalons in the imaging lens and PPLN crystal to be minimized by ratioing the signals of both detection channels. Spectral lines are acquired by DC modulation of the 1560-nm diode laser (triangular waveform at 0.1 to 1 kHz). The pre-amplified signal from the two channels is acquired simultaneously by the use of two analog-to-digital

converter (ADC) data-acquisition cards and then recorded by a notebook PC.

2 Experimental results

The DFG source delivered an optical output of up to $640 \mu\text{W}$ narrow-bandwidth radiation after the PPLN crystal. Due to reflection losses by the collimating CaF_2 lens and Ge filter the spectrometer can operate with a maximum DFG power of $580 \mu\text{W}$ as measured after the Ge filter. In Fig. 2 the DFG power is plotted as a function of the pump power product as measured in front of the crystal. A slope efficiency of $(0.8 \pm 0.04) \text{ mW}/\text{W}^2$ can be deduced from the graph, which corresponds to a DFG conversion efficiency of $0.42 \text{ mW}/(\text{W}^2 \text{ cm})$ for a 19-mm-long crystal. The measured slope efficiency is comparable with a value of $0.76 \text{ mW}/(\text{W}^2 \text{ cm})$ [23] expected from theory. From previous spectroscopic measurements the line width of the system is estimated to be < 60 MHz on a time-scale of 2 min [24]. The long-term line stability over a 24-h period was measured to be $1.5 \times 10^{-2} \text{ cm}^{-1}$. The optical output power available for the field experiment was $300 \mu\text{W}$ with a stability of 20%. This is due to the fact that the fiber amplifiers provide less output power at the elevated and daily varying temperatures to which they are exposed in the field. Long-term power variations in the data channel could reach up to 50% due to misalignment caused by thermal effects in the optical multi-pass cell.

The formaldehyde-concentration measurements reported in this work were obtained over a period of 9 and 5 days, respectively, at two environmental monitoring sites located at Deer Park 2C35/139 [25] operated by the Texas Natural Resource Conservation Commission (TNRCC) and Channelview HRM-3 Haden Road C603/114 [26] operated by the Houston Regional Monitoring Corporation (HRM). Ambient air is sampled 4 m above the ground via a 5-m-long $1/2''$ PFA tube and pumped into the 100-m effective path length multi-pass gas cell. The pressure in the multi-pass detection cell was controlled at (40 ± 0.5) Torr. The airflow provided a complete gas exchange in the $3.3\text{-}\ell$ gas cell every 10 s. The DFG-based spectrometer was maintained at $25\text{--}28^\circ\text{C}$ in an air-conditioned trailer, while the outside temperature typically varied between 24 and 32°C . The sensor was configured to automatically acquire a HCHO-concentration value every 100 s as an average of 2000 measured spectra. During the 9-day operation of the sensor at the Deer Park site there were several outages due to unscheduled work in the trailer by TNRCC personnel. At the Channelview site, 5 days of uninterrupted measurements were performed. The

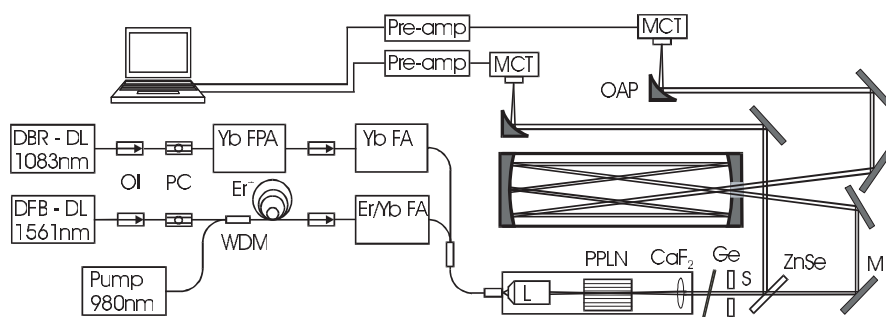


Fig. 1. Schematic of the DFG-based gas sensor used for ambient measurements (OI, optical isolator; DL, diode laser; MCT, Peltier-cooled HgCdTe detector; PC, polarization controller; WDM, wavelength-division multiplexer; PPLN, periodically poled lithium niobate; M, plane mirror; OAP, off-axis parabolic mirror)

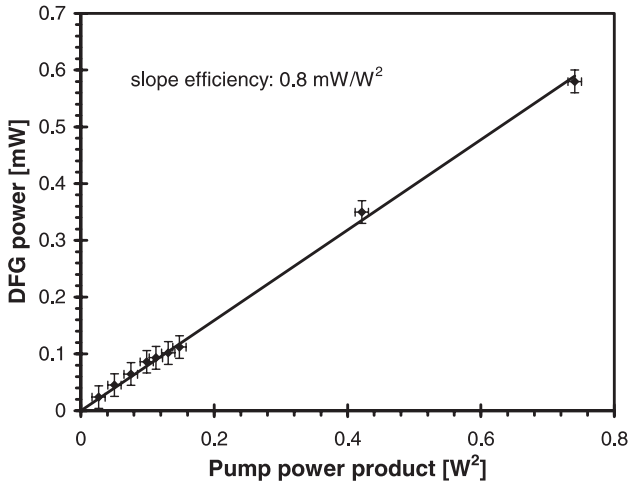


Fig. 2. DFG slope efficiency of the two-stage-amplifier-powered PPLN system. The efficiency, at 0.8 mW/W^2 , is derived from the pump power product plotted as a function of DFG power

data were written to a file and saved on a notebook computer. A modem connection provided convenient remote access to control the sensor operation and to read the data online.

3 Data processing

To detect, quantify, and measure HCHO gas concentration levels, the Lambert–Beer relation $I_\nu = I_{\nu,0} \exp[S(T)g(\nu - \nu_0)NL]$ was utilized, where I_ν is the mid-infrared DFG intensity at frequency ν , measured after propagating a path length L through a medium with an absorbing species of number density N . The strength of the absorption is determined by the temperature-dependent line strength $S(T)$ and the line-shape function $g(\nu - \nu_0)$. The line-shape function describes the temperature- and pressure-dependent broadening mechanism of the fundamental line strength. The temperature dependence of the line strength arises from the Boltzmann population statistics governing the internal energy-level population distribution of the absorbing species.

A given absorption line is characterized by its integrated line strength S in terms of the absorption cross-section, $\sigma(\nu)$:

$$S = \int_0^\infty \sigma(\nu) d\nu, \quad (1)$$

which is independent of pressure (but not of temperature). The line shape depends on sample pressure and temperature. At high pressure and low temperature, collision broadening dominates, resulting in a Lorentzian line shape:

$$\sigma_L(\nu) = \frac{S}{\pi} \frac{\gamma_L}{[(\nu - \nu_0)^2 + \gamma_L^2]}, \quad (2)$$

where γ_L is the half-width at half-maximum (HWHM) of the line shape and ν_0 is the line-center frequency. The line width γ_L varies with pressure p and temperature T approximately according to:

$$\gamma_D = \gamma_{L0} (p/p_0) (T_0/T)^{\frac{1}{2}}, \quad (3)$$

where γ_{L0} is the value of γ_L at a standard pressure of $P_0 = 1013 \text{ hPa}$ and temperature of $T_0 = 296 \text{ K}$. As the sample pressure is reduced the pressure-broadened line width decreases until, at pressures below a few torr, Doppler broadening dominates and the line shape becomes Gaussian:

$$\sigma_D(\nu) = \frac{S}{\gamma_D} [(\ln 2)/\pi]^{\frac{1}{2}} \exp\left[-\frac{(\nu - \nu_0)^2 \ln 2}{\gamma_D^2}\right]. \quad (4)$$

The Doppler width γ_D is given by:

$$\gamma_D = [2kT(\ln 2)/M]^{\frac{1}{2}} \nu_0/c \quad (\text{HWHM}), \quad (5)$$

where M is the molecular mass and c is the velocity of light.

In this work, the optimum sampling pressure for HCHO is a compromise between sensitivity (optimum at high pressure) and selectivity (optimum at low pressure). As the sampling pressure is reduced, the sensitivity does not decrease significantly below the value at atmospheric pressure until a point at which Lorentzian and Doppler line widths are equal (typically between 10 and 50 Torr). This is the pressure at which this HCHO sensor was normally operated (i.e. 40 Torr). In this pressure range the line shape can be described as a convolution of Lorentzian and Doppler line shapes known as a Voigt profile. This can be expressed in terms of a complex error function, but since this is difficult to evaluate, it is often convenient to use an approximation first reported by Whiting [27] and further developed by Brassington [28]:

$$\sigma_V(\nu) = \sigma_V(\nu_0) \left\{ (1-x) \exp(-0.693y^2) + x / (1+y^2) + (*) \right\}, \quad (6)$$

where

$$(*) = 0.016(1-x)x \left[\exp(-0.0841y^{2.25}) - 1 / (1 + 0.0210y^{2.25}) \right]$$

with $x = \gamma_L/\gamma_V$ and $y = |\nu - \nu_0|/\gamma_V$. The line width γ_V of the Voigt profile is given approximately by:

$$\gamma_V = 0.5346\gamma_L + (0.2166\gamma_L^2 + \gamma_D^2)^{\frac{1}{2}} \quad (\text{HWHM}) \quad (7)$$

and $\sigma_V(\nu_0)$, the cross-section at the line center, is given by:

$$\sigma_V(\nu_0) = S / [2\gamma_V (1.065 + 0.447x + 0.058x^2)]. \quad (8)$$

The Voigt profile tends to a Lorentzian profile at high pressure ($x = 1$) and to a Doppler profile at low pressure ($x = 0$) and is thus the general form of the line shape. This approximation accurately describes the full Voigt convolution to within 1%–3% depending on the location in the profile. For this experiment, the Voigt-profile approximation given by (6)–(8) was used employing the Levenberg–Marquardt non-linear least-squares fitting algorithm. The fitting routine was written in Labview[®] code. The fitting algorithm first calculates the natural logarithm of the ratio of the detected intensity in the data channel versus intensity in the reference channel $I_\nu/I_{\nu,0}$. This ratio gives the logarithm of the transmittance of the signal. Due to power changes in both data and reference channels within each scan, even after normalization of the data the baseline is not flat and must be modeled.

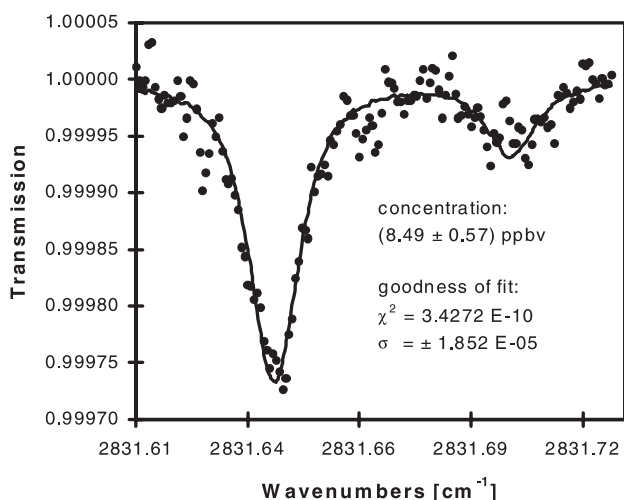


Fig. 3. Normalized HCHO absorption spectrum (single data points) obtained in the field and a 2-line Voigt fit with the Doppler width fixed at $1.436 \times 10^{-2} \text{ cm}^{-1}$ (FWHM) as given by HITRAN [29]

Therefore, the algorithm then simultaneously performs a Levenberg–Marquardt nonlinear least-squares fit to a cubic baseline and two adjacent formaldehyde ro-vibrational transitions. A typical normalized spectrum acquired in the field with fitted baseline (dots) and a modeled 2-line Voigt profile (solid line) are shown in Fig. 3. The modeled Voigt profile has a χ^2 error of 3.4272×10^{-10} indicating a concentration and uncertainty of (8.49 ± 0.57) ppb V. The measured uncertainty (σ) of 0.57 ppb V is larger than the detection limit of 0.32 ppb V and is due to the noise induced by field conditions. The molecular HCHO transitions used in this work occur at $2831.6417 \text{ cm}^{-1}$ and $2831.6987 \text{ cm}^{-1}$, respectively. These lines were selected because they are free from interference of other molecular transitions, in particular H_2O and CO_2 [21]. The bigger peak enables low-concentration measurements of formaldehyde, whereas the smaller peak provides additional information that can be used to improve the precision and accuracy of the HCHO-concentration measurements. Since the a priori distance between the peaks as well as their locations are given by the HITRAN [29] spectroscopic database, this allows the calculation of the frequency tuning per point in the algorithm. The line intensities S of both peaks as well as their ratio, and the Voigt line width $2\gamma_V$ of $1.436 \times 10^{-2} \text{ cm}^{-1}$ (full-width at half-maximum (FWHM)) are also known from HITRAN. To determine the concentration of the HCHO sample gas, Lambert–Beer’s law must be solved for N , where

$$N = \ln(I_{v,0}/I_v) S(T) g(v - v_0) L. \quad (9)$$

In this experiment, the effective optical path length L is 100 m. To obtain the concentration c in ppb V, N is used in the following equation:

$$c[\text{ppb V}] = 10^9 NT[\text{K}] / (N_L p[\text{hPa}]), \quad (10)$$

where the Loschmidt number $N_L = 9.68 \times 10^{18}$ relates N (total number of molecules) to volume at the specified temperature and pressure.

4 Performance

To determine the best time resolution of the DFG spectrometer, an Allan variance measurement shown in Fig. 4 was performed in the laboratory [21, 30]. This measurement was performed using the Herriott multi-pass cell open to ambient laboratory air containing a calculated HCHO concentration of 5 ppb V. Absorption spectra were collected in packets of 100 averages, which represents a data-integration time t of 1 s and then are subsequently summed into bigger packages in order to simulate an increasing integration time. Figure 4 shows the variance of the acquired spectra compared to a modeled Voigt profile depending on the integration time of the measurement. Figure 4 indicates that the optimum integration time τ_{opt} is 20 s, which gives an optimum standard deviation of $\sigma_{\text{opt}} = 0.32$ ppb V (as marked with an arrow). This integration time represents an optimum number of 2000 averages. This was the number that was used to acquire the formaldehyde-concentration values in the field experiments. At shorter time periods the Allan variance increases inversely proportionally to τ due to the dominant influence of white noise (marked with a dashed line).

The relation between DFG power, noise, and precision of the HCHO-concentration values was investigated. Figure 5 shows the signal-to-noise ratio (SNR) of the spectra as a function of DFG power, from which it is evident that there is a linear relation between power and signal-to-noise ratio up to 18- μW power. At higher power levels the SNR is independent of the DFG power incident on the detector. A maximum SNR of 37 is achievable with this sensor, which results in a detection limit of 0.32 ppb V at a concentration level of 7.0 ppb V.

5 Discussion

The described sensor was used for automated monitoring of formaldehyde in ambient air at two field sites, Deer Park and Channelview, in the Greater Houston area as shown

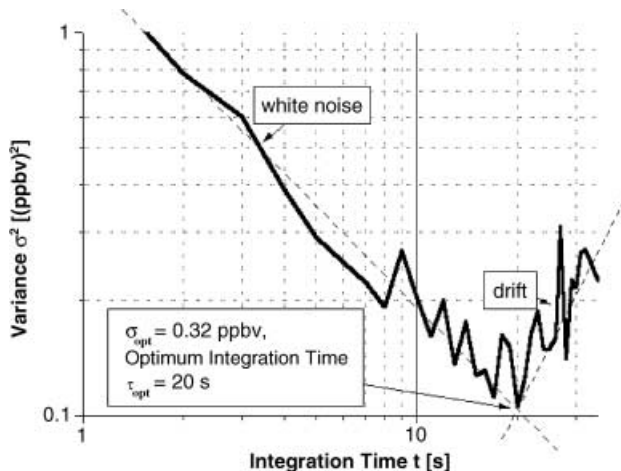


Fig. 4. Allan variance calculated from a measurement of HCHO with a concentration of 5 ppbV. The variance at different integration times was obtained in 100 sample bins and a subsequent fitting of the spectra to a modeled Voigt profile. The *dashed* and *solid* lines indicate an optimum integration time of $\tau_{\text{opt}} = 20$ s, which yields a detection limit expressed in terms of the standard deviation $\sigma_{\text{opt}} = 0.32$ ppbV

in Fig. 6. The HCHO-concentration data in ambient air obtained in the 9-day campaign at the Deer Park 2C35/139 site are depicted in Fig. 7a. A 15-min rolling average (solid line), together with the measured concentration values (dots), is plotted. For comparison, results of simultaneously performed 24-h averaging measurements with the established wet-chemical *o*-(2,3,4,5,6-pentafluorobenzyl) hydroxylamine (PFBHA) technique are shown as horizontal bars. The general agreement between the two trace-gas detection methods is apparent. Concentrations measured by the DFG system vary between 0 and 20 ppb V, although most values range from 2 to 8 ppb V. On a short time-scale (1 h) there is a variation in the HCHO concentration of about 2–4 ppb V, and only 1–2 ppb V when considering the rolling average. Hence it is evident that there is no apparent formaldehyde-concentration change occurring on a time-scale of one (or more) hours, even up to a 24-h period, especially considering the fit precision of 0.57 ppb V calculated from Fig. 3. Thus, the DFG meas-

urements, on the order of minutes, add considerably to the understanding of HCHO atmospheric chemistry. The fluctuations that occur on such a small time-scale are seen only by the DFG technique, and are hidden by day-long wet-chemistry sampling methods. Figure 7b shows the ambient ozone concentrations measured by the TNRCC instrumentation in the same time period. The correlation in the data shown in Fig. 7a and b confirms the intertwined sources and atmospheric chemistry of ozone and formaldehyde. The sharp increase of both formaldehyde and ozone on 18 June 2000 was detected immediately after a heavy thunderstorm. These

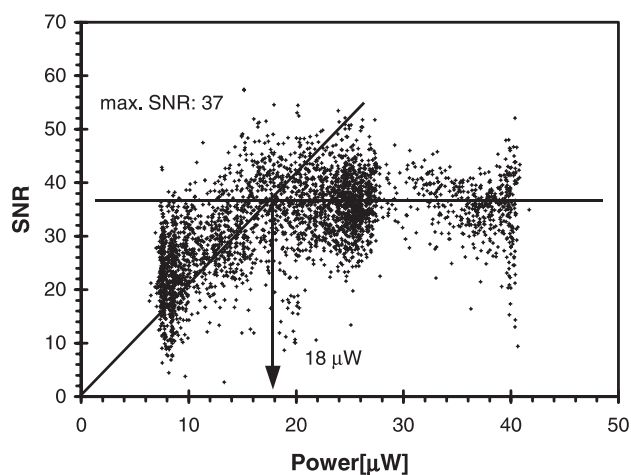
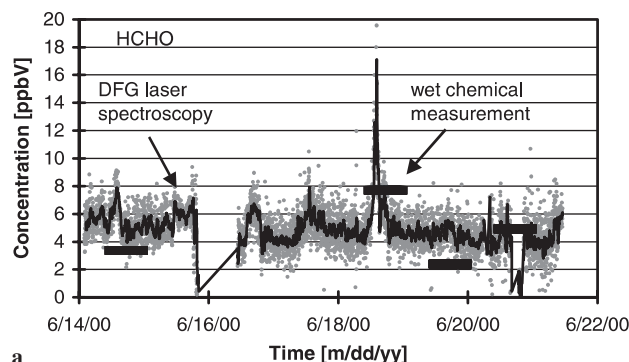


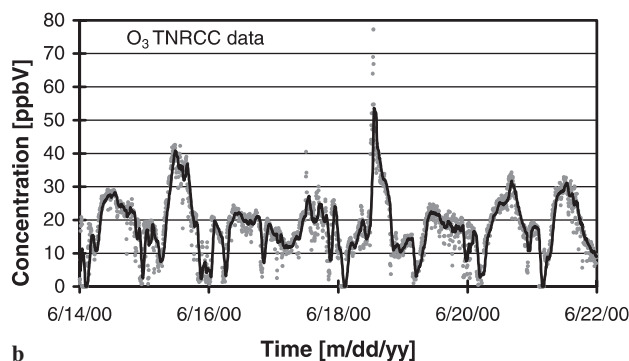
Fig. 5. Relationship between DFG power and the SNR of HCHO spectra. A linear relationship between power and SNR exists up to 18 μW . At higher powers the SNR remains constant at a value of 37 independent of any further power increases



Fig. 6. Map of the Greater Houston area indicating locations of the two monitoring sites, Deer Park and Channelview. These sites are located near the Houston Ship Channel, a major industrial center



a



b

Fig. 7. a Time-resolved HCHO-concentration measurements taken over a nine-day period [6–20 June 2000] at the Deer Park monitoring station. The HCHO measurements are indicated as follows: DFG laser spectroscopy, *dots*; a 15-point rolling average, *solid line*; and wet-chemical analysis, *bars*. b Related ozone concentrations, also taken at Deer Park, as measured by the TNRCC during the same time period

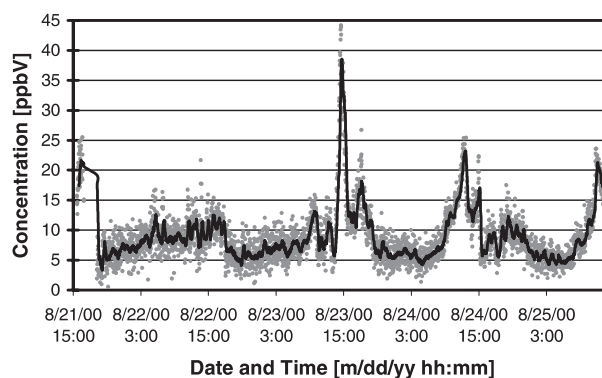


Fig. 8. Five days of continuous HCHO data obtained at the Channelview monitoring station, with the DFG laser spectroscopy data (*dots*) together with 15-point rolling average (*solid line*)

figures seem to suggest the importance of real-time measurements of HCHO, since the correlation between HCHO and simultaneously measured ozone can be studied.

The data from the Deer Park site are from an urban area with environmentally determined HCHO-concentration levels. In comparison, the measurements carried out at Channelview HMR-3 show an HCHO history at an emission site in a predominantly industrial area. As depicted in Fig. 8, HCHO concentrations reach up to 45 ppb V in the early afternoon, which indicates that there might be a local formaldehyde source, while the background concentration is ~ 5 ppb V.

6 Conclusions

Formaldehyde-concentration measurements using direct absorption laser spectroscopy have proved to be a sensitive and effective method for online trace-gas monitoring. While the accuracy of the determined concentrations is comparable with results from conventional wet-chemical techniques, the described DFG sensor offers excellent time resolution on the order of seconds and permits unattended continuous operation for long periods of time. The inherent maintenance-free design of a tunable infrared DFG-based diode-laser spectrometer and the capability of remotely controllable computerized operation make such instrumentation a convenient, robust tool for mobile trace-gas detection.

Acknowledgements. This work was funded by the Gulf Coast Hazardous Substance Research Center, the Texas Advanced Technology Program, NASA, the Welch Foundation, and the National Science Foundation.

References

1. National Research Council: *Rethinking the Ozone Problem in Urban National and Regional Air Pollution* (National Academy, Washington DC 1991)
2. W.P.L. Carter: *J. Air Waste Manage. Assoc.* **44**, 881 (1994)
3. E. Grosjean, D. Grosjean, M.P. Fraser, G.R. Cass: *Environ. Sci. Technol.* **30**, 2687 (1996)
4. M.P. Fraser, E. Grosjean, D. Grosjean, R.A. Rasmussen, G.R. Cass: *Environ. Sci. Technol.* **30**, 1731 (1996)

5. P.K. Dasgupta, S. Dong, H. Hwang, H.C. Yang, Z. Genfa: *Atmos. Environ.* **22**, 949 (1991)
6. A. Fried, B. Henry, B. Wert, S. Sewell, J.R. Drummond: *Appl. Phys. B* **67**, 317 (1998)
7. A. Fried, S. Sewell, B. Henry, B.P. Wert, T. Gilpin: *J. Geophys. Res.* **102**, 6253 (1997)
8. D.D. Nelson, M.S. Zahnriser, J.B. McManus, C.E. Kolb, J.L. Jimenez: *Appl. Phys. B* **67**, 433 (1998)
9. P. Werle: *Spectrochim. Acta A* **54**, 197 (1998)
10. D.R. Lawson, H.W. Biermann, E.C. Tuazon, A.M. Winer, G.I. Mackay, H.I. Schiff, G.L. Kok, P.K. Dasgupta, K. Fung: *Aerosol Sci. Technol.* **12**, 64 (1990)
11. T. Gilpin, E. Apel, A. Fried, B. Wert, J. Calvert, Z. Genfa, P. Dasgupta, J. Harder, B. Heikes, B. Hopkins, H. Westberg, T. Kleindienst, Y.N. Lee, X. Zhou, W. Lonneman: *J. Geophys. Res.* **102**, 21 161 (1990)
12. A. Vairavamurthy, J.M. Roberts, L. Newman: *Atmos. Environ.* **26**, 1965 (1992)
13. Y. Mine, N. Melander, D. Richter, D.G. Lancaster, K.P. Petrov, R.F. Curl, F.K. Tittel: *Appl. Phys. B* **65**, 771 (1997)
14. D.G. Lancaster, D. Richter, R.F. Curl, F.K. Tittel: *Appl. Phys. B* **67**, 339 (1998)
15. U. Simon, F.K. Tittel: *Infrared Phys. Technol.* **36**, 427 (1995)
16. D. Richter, D.G. Lancaster, R.F. Curl, F.K. Tittel: *Appl. Opt. B* **67**, 347 (1998)
17. S. Friedfeldt, M. Fraser, D.G. Lancaster, D. Leleux, D. Rehle, F.K. Tittel: *Geophys. Res. Lett.* **27**, 2903 (2000)
18. D.G. Lancaster, D. Richter, F.K. Tittel: *Appl. Phys. B* **67**, 339 (1998)
19. L. Goldberg, J.P. Kaplow, D.A.V. Kliner: *Opt. Lett.* **24**, 673 (1999)
20. D.G. Lancaster, D. Rehle, D. Leleux, F.K. Tittel: *Conference on Lasers and Electro-Optics (OSA Tech. Digest)* (Optical Society of America, Washington DC 2000) p. 514
21. D.G. Lancaster, A. Fried, B. Wert, B. Henry, F.K. Tittel: *Appl. Opt.* **39**, 4436 (2000)
22. M. Seiter, M.W. Sigrist: *Infrared Phys. Technol.* **41**, 259 (2000)
23. P. Canarelli, Z. Benko, R.F. Curl, F.K. Tittel: *J. Opt. Soc. Am. B* **9**, 197 (1992)
24. D.G. Lancaster, D. Richter, R.F. Curl, F.K. Tittel: *Opt. Lett.* **24**, 1744 (1999)
25. http://www.tnrcc.state.tx.us/cgi-bin/monops/site_photo?35
26. http://www.tnrcc.state.tx.us/cgi-bin/monops/site_photo?603
27. E.E. Whiting: *J. Quantum Spectrosc. Radiat. Transfer* **8**, 1379 (1968)
28. D.J. Brassington: *Spectroscopy in Environmental Science*, ed. by R.J.H. Clark, R.E. Hester (Wiley, New York 1995)
29. L.S. Rothman, C.P. Rinsland, A. Goldman, S.T. Massie, D.P. Edwards, J.M. Flaud, A. Perrin, C. Camy-Peret, V. Dana, J.-Y. Mandin, J. Schroeder, A. McCann, R.R. Gamache, R.B. Wattson, K. Yoshino, K.V. Chance, K.W. Jucks, L.R. Brown, V. Nemtchinov, P. Varanasi: *J. Quantum Spectrosc. Radiat. Transfer* **60**, 665 (1998)
30. P. Werle, R. Muecke, F. Slemr: *Appl. Phys. B* **57**, 131 (1993)